Research Insights

4D printing and programming of continuous fibre-reinforced shape memory polymer composites

Mohammadreza Lalegani Dezaki , Mahdi Bodaghi [*]

Department of Engineering, School of Science and Technology, Nottingham Trent University, Nottingham NG11 8NS, UK

ARTICLE INFO

ABSTRACT

This study demonstrates the use of fused filament fabrication (FFF) 4D printing (4DP) to print programmable continuous fibre-reinforced composite (CFRC) structures with exceptional strength and eco-friendly features. This research focuses on bio-shape memory polymer composites (SMPCs) and employs experiments to fabricate lightweight CFRC parts using FFF technology. Different types of continuous fibres, including carbon fibre (CF), aramid fibre (AF), and fibreglass (FG), are incorporated into a biopolymer matrix made of biodegradable polylactic acid (PLA). The study evaluates microstructure, mechanical properties, and shape memory properties of SMPCs, employing techniques like cold and hot programming. Continuous fibres significantly enhance mechanical properties, increasing strength by over 1027.5 % in tensile tests and nearly 497.3 % in three-point bending tests. The research also addresses shape recovery and fixity ratios in 4D-printed SMPCs, finding a decrease when continuous fibres are incorporated into PLA. Notably, FGPLA specimens achieve the highest shape recovery ratio of approximately 95 ± 1 % after pure PLA. These findings highlight the potential of 4D-printed CFRCs in various applications, from human-material interaction to mechanical and biomedical fields. They contribute to sustainability by reducing material consumption and waste, demonstrated through the creation of reusable and lightweight items like hooks, lockers, finger splints, and meta-composites.

1. Introduction

4D printing (4DP) is an advanced method of additive manufacturing [1]. It's used to create dynamic structures that can change shape and structure when exposed to certain environmental factors [2]. This technology allows materials like thermoplastics to be programmed to transform over time. Shape memory polymers (SMPs) and shape memory polymer composites (SMPCs) are materials that are often used in 4D-printed actuators and structures that can change their shape and configuration [3,4]. They show great potential for applications from engineering to medical fields [5–7]. They can maintain a predefined shape and then return to their original, permanent shape when triggered by external factors [8].

The fused filament fabrication (FFF) approach stands out as the most popular among 3D printing processes, mostly due to its affordability in terms of printer equipment and the accessibility of a large variety of affordable SMPs and SMPCs [9,10]. FFF 3D printers are widely used in a variety of sectors, particularly for fast prototyping [11–13]. Thermoplastic SMPs in the FFF process offer benefits in terms of affordability

and ease of printing, yet they typically exhibit limitations in terms of their mechanical strength and performance [14–16]. Continuous fibre printing has been a key approach for enhancing the mechanical characteristics of SMPs produced by FFF 4DP [17,18]. The procedure of 3D printing of continuous fibre-reinforced composites (CFRCs) involves incorporating continuous fibres into the material through a combination of in-situ impregnation and fibre tension in FFF process [19]. CFRCs improve mechanical properties while reducing material usage and promoting lightweight products [20–22].

The potential uses of SMPCs have been expanded by several investigations that have focused on 4DP CFRCs [23,24]. Research works also focused on shape recovery and shape fixity of printed CFRCs metamaterials and their performance [25–27]. Zeng et al. [28] investigated the electro-induced shape memory effect (SME) of the 4D-printed continuous carbon fibre (CF) reinforced polylactic acid (PLA)-based composites by conducting tests involving electric heating to observe the shape recovery process. The stability and feasibility of the resistance heating approach were demonstrated by the results, which showed a shape recovery rate of more than 95 % [29]. Dong et al. [30]

investigated the influence of both printing and structural parameters on the mechanical properties and shape memory capabilities of the printed CFRCs. The results from experiments demonstrated that even a modest inclusion of 3.8 % fibre in the composite led to a significant increase in tensile strength by more than 300 %. However, introducing more fibre had an adverse impact on the composite's ability to recover its shape, thereby negatively affecting its shape-changing properties.

Moreover, Zhou et al. [31] introduced a co-extrusion 4DP technique that incorporates continuous metallic fibres into thermoplastic SMPs. This integration established an electrical heating pathway within the polymer matrix. The heating rate achieved for SMPCs using this method was 70 times faster. Chen et al. [32] used FFF to fabricate SMPCs comprised of continuous CF and reinforced PLA. This composite exhibited remarkable qualities such as high strength, potent shape recovery force, swift response to low-voltage stimuli, and outstanding electrothermal SME. Under electrical thermal stimulation, most specimens achieved a shape recovery ratio of 90 %. Also, Yang et al. [33] found out the distinct bending characteristics of this cost-effective printed active composite across various physical states. The noteworthy magnitudes of maximum deformation and deformation force measuring 7 mm and 100 mN for CF/PLA specimens, and 10 mm and 200 mN for CF/polyether-ether-ketone specimens highlighted the potential application of this dual-layer SMPCs and the 4DP technique in

areas such as biomimetic sensors, actuators, transducers, and artificial muscles.

While prior research has extensively examined the progression and analysis of SMPCs strengthened by continuous fibres [34–36], these inquiries predominantly revolved around the utilization of such continuous fibres to strengthen the mechanical attributes of 4D-printed meta-composite structures. Additionally, they aimed to evaluate the efficacy of SMPCs in terms of critical factors like shape recovery and the SME. However, it's important to highlight that these earlier investigations have often overlooked a significant aspect in terms of fibre comparison in SMPC printing. These roles are played by fibres like aramid fibre (AF), fibreglass (FG), and CF when integrated as reinforcing agents within 4D-printed PLA smart materials. The examination of reusability and lightweight properties in 4D-printed SMPCs remains unexplored. Exploring the potential reduction in structural weight and material usage will pave the way for sustainable and environmentally friendly design practices. This omission underscores a valuable research gap, underscoring the need to delve into the unexplored terrain of these specific fibre reinforcements.

The novelty aspect of this research lies in the investigation of FFF 4D-printed CF, FG, and AF in conjunction with a biodegradable PLA matrix. The main goal is to understand the shape memory properties in printed SMPCs via cold and hot programming while analysing the

Fig. 1. 4DP of SMPCs showcasing their role in sustainability and demonstrating applications across industries. The transformative potential of 4DP technology in revolutionizing material engineering and design.

microstructure and mechanical properties of printed CFRCs. This method results in reduced material usage and waste, yielding a final product that is both lighter and stronger, ultimately enhancing its overall quality. It also allows for the reusability of 4D-printed objects due to the shape recovery feature, aligning with circular economy principles for eco-friendly, long-lasting manufacturing. This technique is crucial for sustainability as it minimizes material usage in printing while improving mechanical strength. Additionally, shape fixity and shape recovery in fibre-infused specimens are evaluated under identical printing conditions. A detailed examination of the shape memory

responses of 4D-printed SMPCs for a deeper understanding is conducted as well. This includes a thorough analysis of microscopic and SEM images of fractured specimens and microstructure with integrated fibres. Findings highlight the potential of SMPCs to revolutionize various fields including soft actuators, human-material interaction, medical devices, and cellular structures. Fig. 1 illustrates the application concept achievable through this method. The ability to reuse printed structures minimizes material waste and consumption during the printing process. These printed structures are both lightweight and sufficiently strong. In essence, this technique promotes sustainability through its highlighted
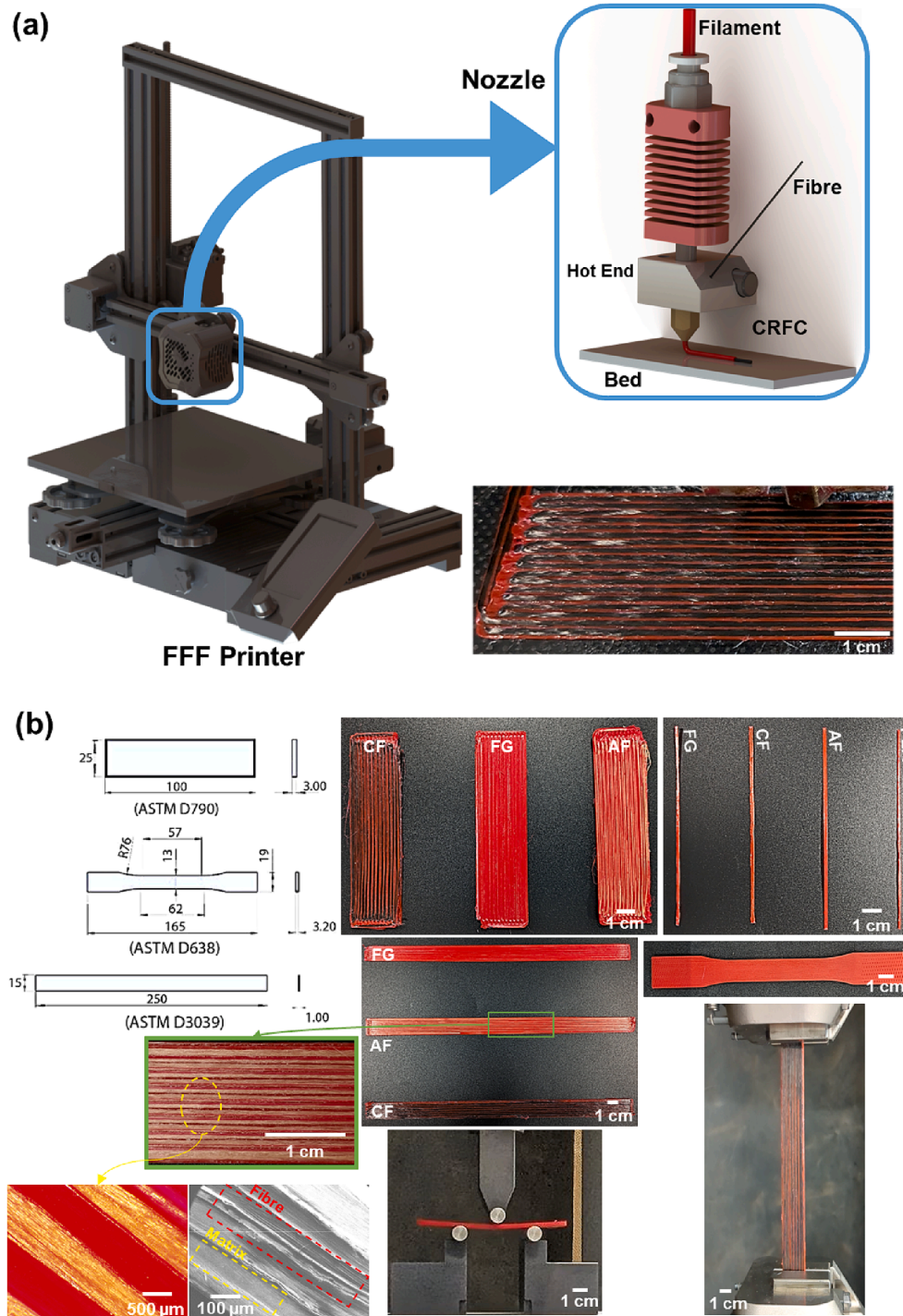
Fig. 2. (a) The schematic depicts a diagram of an FFF printer and its nozzle utilized for printing CFRCs, along with an illustration of printing composite specimens. (b) Images of CFRC beams and samples fabricated following ASTM standards for mechanical tests.

attributes.

2. Materials and methods

2.1. Materials

The matrix material utilized in this study needs to possess SME properties to achieve the capability of changing shape. PLA is extensively employed in 4DP due to its significant SME characteristics [37]. Moreover, PLA filament constitutes an environmentally friendly thermoplastic polymer sourced from renewable materials [38]. PLA is known for its user-friendly nature, often requiring minimal exertion to create high-quality components, particularly when using an FFF 3D printer [39]. In this research, we utilize red PLA filament with a 1.75 mm diameter and a density of 1.24 g/cm3, obtained from 3DGence, for all the printed specimens. Thermoplastics currently exhibit suboptimal mechanical properties. As a result, CFRCs have been employed to enhance the mechanical attributes of printed products. A range of fibre reinforcements are suitable for printing purposes. CF, AF, and FG are all amenable to FFF printing. The fibres used in this study are all procured from Markforged, and no pre- or post-processing is conducted on the fibres. The fibres have a uniform diameter, each measuring 0.36 mm. Specific fibre properties are in the company's datasheets [40–42].

2.2. Extruder development and printing process

This section gives a thorough explanation of the manufacture of CFRCs and the design extruder developed for FFF printers. This work employs a Creality Ender 3 V2 3D printer. The printer has been assembled, and its extruder has been appropriately modified for the purpose of this study. The extruder is in charge of integrating extended continuous fibres and molten plastic at the same time so that they may later be deposited together. In this regard, predetermined designs are followed to build the extruder [43,44]. A brass nozzle, an aluminium hot block, heaters, and an aluminium heat sink are just a few of the components that make up the ensemble of the planned extruder, as shown in Fig. 2a. The extruder of the Creality Ender 3 V2 has been adapted, and the hot end has been redesigned and constructed to enable the printing of CFRCs. This extruder has two inlets, the first of which is for inserting unprocessed PLA plastic filament and the second of which is for introducing continuous fibre. The fibre moves through the hot block within a slender stainless-steel pipe, ensuring that the fibre doesn't encounter the molten plastic until it reaches the nozzle's tip.

The Teflon PTFE tubing that surrounds the stainless-steel pipe acts as insulation, preventing direct contact between the pipe and the block. Therefore, the stainless-steel pipe is efficiently kept from overheating thanks to the PTFE pipe, which has a thermal conductivity of 0.25 W/ (m.K). This configuration is essential for avoiding nozzle blockage. The plastic filament is extruded while printing is taking place, stretching the fibre originating from the printed area of the fibres. This force protects the fibre against deformation along the print path, which results from motion between the nozzle and the print bed. The ratio of molten plastic to fibres is equal for all samples since the extruder's speed controls the feed rate of the plastic filament.

All specimens in this study are printed using constant printing

Table 1
Printing parameters of CFRCs.

Parameters	Value
Nozzle Diameter (mm)	1.5
Layer Thickness (mm)	0.25
Printing Speed (mm/s)	15
Infill Density (%)	100
Printing Pattern	Linear
Nozzle Temp. (°C)	210
Bed Temp. (°C)	60

parameters as shown in Table 1. The designed extruder with a diameter of 1.5 mm is used to create all test samples without clogging issues [45,46]. The SolidWorks software is used to design the geometry of these prototypes. The specimen's shape is then saved as a stereolithography file (STL) and loaded into the slicing Slic3r program where processing settings are adjusted. Due to the 180° printing route shift at both ends of the length direction, a drop in printing speed is imposed for flat CFRCs. This modification gives the requisite fibre tension plenty of time to grow and for solidification to occur.

To further explain, utilising the G-code approach in numerical control, numerous aspects like the nozzle's feed speed, the length of the extrusion pause during fibre redirection, and route programming to prevent fibre entanglement are taken into consideration. A single layer's printing route is adhered to while arranging material layers along each composite part's thickness. Utilising the G-code approach in numerical control, numerous aspects like the nozzle's feed speed, the length of the extrusion pause during fibre redirection, and route programming to prevent fibre entanglement are taken into consideration.

2.3. Dynamic mechanical analysis (DMA)

The SME of 4D-printed SMPCs is related to two crucial thermodynamic variables, the storage modulus and the glass transition temperature (T_g). To evaluate the material's ensuing shape memory behaviour, several characteristics must first be assessed. Analysis of the effects of fibre incorporation on the storage modulus and T_g of the used semicrystalline PLA is required. In order to perform dynamic thermomechanical analysis on 4D-printed pure PLA and CFRC specimens, a dynamic thermo-mechanical analyser (DMA 8000 PerkinElmer) is employed in this study. A beam sample is printed with 30 mm in length, 8 mm in width, and 1 mm in thickness. At a frequency of 1 Hz and a rate of 5 °C/min, the temperature is raised from 30 °C to 80 °C.

2.4. Mechanical properties

The CFRC samples' mechanical characteristics are assessed utilizing a versatile mechanical testing apparatus, specifically the Shimadzu AG-X plus machine, which is fitted with a 50 kN load cell and monitored specimen movement using an optical camera. The dimensions of the tensile specimens for pure PLA and CFRCs are chosen according to the standards ASTM D638 and ASTM D3039 with a speed of 2 mm/min, respectively [47,48]. Similarly, beams with dimensions of 100 mm in length, 1.5 mm in width, and 0.5 mm in thickness are employed for the tensile test. This aims to explore the impact of a layer of fibre within a PLA matrix on mechanical properties. Furthermore, samples are produced to examine their characteristics through a three-point bending examination. The bending specimens' dimensions are selected in line with ASTM D790 with a speed of 2 mm/min and a span length of 40 mm [49]. The required qualities are tested on a total of five samples, and the average values for each are presented. All the samples are printed in the longitudinal direction to maximize their strength. Fig. 2b shows the test specimens and the final printed samples. The calculation of stress and strain is based on ASTM D790 as follows:

$$\sigma_f = \frac{3FL}{2bd^2} \tag{1}$$

$$\epsilon_f = \frac{6Dd}{L^2} \tag{2}$$

In this context, F represents the force causing bending, L denotes the distance between supports, b stands for the width of the test sample, d represents its thickness, and D is the maximum deflection of the centre of the beam.

2.5. Scanning electron microscope (SEM) and optical imaging

A scanning electronic microscope (JSM-7100 F LV FEG) and Leica ICC50 W microscope are used to examine the phase structure of the CFRCs and evaluate the fracture and fibre integration within the PLA matrix. After the tests, the printed samples' interface shapes and broken cross-sectional views are analysed. The purpose of this investigation is to assess the printed composite's overall bonding strength as well as how effectively the individual components are integrated.

2.6. Shape memory properties

It may be deduced that the basic idea of SME includes the production of thermal energy because the majority of SMPCs are triggered by heat, which is created by the application of external heat. The shape recovery of the printed samples shape under thermal stimulation is evaluated through the application of both cold and hot programming techniques (see Fig. 3a) [50,51]. To explore the SME of the printed samples, every specimen is designed using SolidWorks. Simple beams with a size of 50 mm length, 1.5 mm width, and 0.5 mm thickness are designed and printed. The aim is to find out the effects of fibre on SME of PLA matrix. A beam is fabricated to assess the impact of a single layer of fibre within a PLA matrix. To achieve this, a two-layer printing method is employed. As depicted in Fig. 3b, the initial layer comprises PLA infused with fibre. Subsequently, the fibre is manually cut, and the second layer solely consists of a PLA matrix. This approach effectively encases the fibre within the initial matrix layer, preventing fibre breakage and ensuring robust bonding. A set of 10 samples is tested for CFPLA, AFPLA, and FGPLA, respectively.

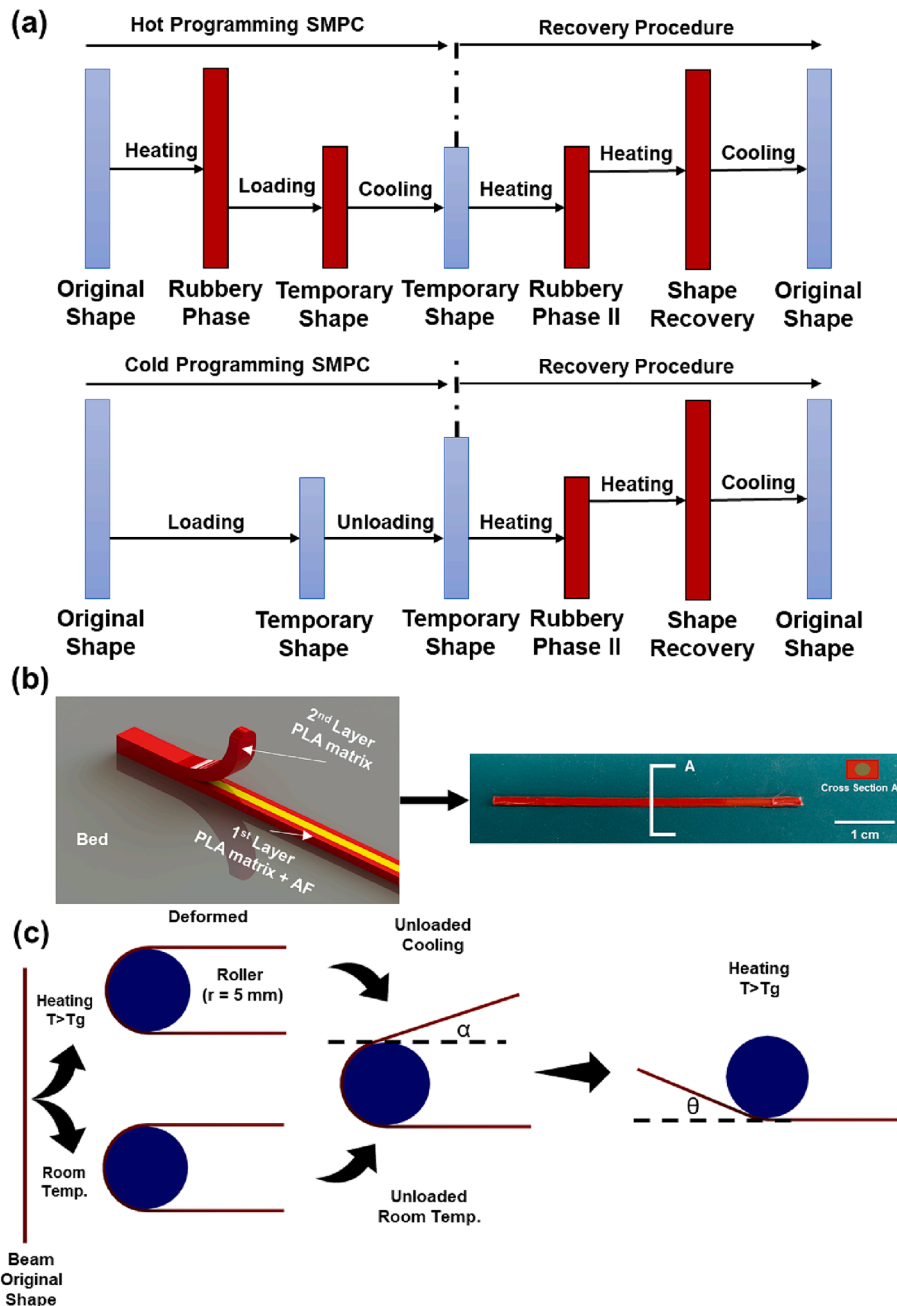Fig. 3c depicts the procedure for programming shape memory in

Fig. 3. (a) The process of programming SMPC in both cold and hot conditions. (b) Image of the printing procedure and printed SMPC with a cross-sectional view. (c) The steps involved in cold and hot shape programming and recovery.

detail. The process of deforming through hot programming occurs within a heat gun that is temperature-controlled and set above the T_g. Following this, the deformed specimens are cooled to establish their shape stability. Conversely, during cold programming, the beams are deformed at room temperature, and subsequently, the force is released to ensure their shape stabilization. Eventually, all the beams programmed through both hot and cold methods are heated above T_g to return to their original forms. The shape fixity and recovery ratio can be computed using Equations (3) and (4).

$$R_f = Shape\ fixity\ ratio = \frac{\theta_{deformed} - \alpha}{\theta_{deformed}} \times 100\% \tag{3}$$

$$R_r = Shape\ recovery\ ratio = \frac{\theta_{deformed} - \theta_{unrecovered}}{\theta_{deformed}} \times 100\% \tag{4}$$

The sample's residual deformation that does not reverse after the delivery of a stimulus is referred to in this context as the angle $\theta_{unrecovered}$. The greatest angle to which the sample is distorted and momentarily kept in situ is represented by the $\theta_{deformed}$ (see Fig. 3c unloaded section). In the experiment, the mean values for both angles are calculated. The beams are secured at one end and positioned vertically. The process of heating is carried out using a heat gun at a predetermined temperature. The sequence of shape recovery is captured and documented using a camera, PASCO software, and FLIR E5-XT thermal imager from FLIR. Also, A Keithley 2110 bench multimeter equipped with a wired thermocouple is employed to gauge the temperature of beams during their shape restoration process.

3. Results and discussion

3.1. Mechanical properties

The efficiency of the developed extruder and the performance of fibres in CFRCs are evaluated by producing standard tensile and bending test specimens, as well as simple beams, using both pure PLA and PLA enhanced with continuous fibres. The printing accuracy of the printer to print specimens is ± 0.25 mm. We have conducted the fibre content measurement by adhering to the outlined steps. The fibre is continually dispersed throughout the printing head's tool path after being extruded together with the melted plastics during the printing process. The weight of the fibre within the specimen is determined by multiplying the weight per unit length, while the length of the tool path automatically determines the length of the fibre [52]. As a result, the weight ratio of the fibre to the composite specimen is the fibre content. Layer thickness is a reflection of the tool path and unit volume of the extruded plastic matrix, which dictates the fibre content in the printed CFRCs. Therefore, the determination of fibre content for printed specimens is essential. In the case of CFPLA, AFPLA, and FGPLA, the calculated fibre content stands at 18.11 %, 17.98 %, and 17.86 %, respectively. This metric serves as a crucial indicator of the composite's composition, directly influencing its mechanical properties and performance characteristics.

Fig. 4a displays the results of the tensile tests conducted on printed PLA and CFRCs, following ATSM D638 and D3039 standards. All samples are printed under consistent conditions, with the same fibre content. The results clearly indicate a significant increase in strength when using printed CFRCs. A comparison between CFRCs and pure PLA reveals a notable enhancement in mechanical properties with the incorporation of continuous fibre [53,54]. CFPLA exhibits the highest strength in comparison to FGPLA and AFPLA with an average value of 461 MPa. However, it's worth noting that the samples tend to develop cracks sooner due to the inherent brittleness of continuous CF [55]. Meanwhile, AFPLA and FGPLA display a strength of approximately 335 ± 5 MPa, with FGPLA exhibiting notably higher strain up to the point of failure compared to CFPLA and AFPLA. Additionally, tensile tests are conducted on simple beams with dimensions of 100 mm in length, 1.5 mm in width, and 0.5 mm in thickness. A layer of fibre/PLA is printed

with the objective of assessing the impact of this single fibre layer on mechanical properties. Fig. 4b illustrates the results of the tensile tests performed on pure PLA and CFRC beams. The findings mirror those of the ASTM specimens. Notably, the incorporation of a single layer of FG within the PLA matrix demonstrates slightly higher strength compared to AFPLA in this case.

Furthermore, three-point bending tests are conducted to assess the performance of the printed samples (refer to Fig. 4c). As observed in the tensile tests, CFPLA exhibits superior mechanical properties compared to AFPLA, FGPLA, and pure PLA, averaging 222 MPa. Pure PLA reaches a maximum stress value of 37 MPa, followed by AFPLA with an average stress value of 102 MPa. The CF and FG specimens exhibit progressive cracking due to the stiffer and more brittle nature of these fibres in comparison to AF. The CFPLA specimens exhibit superior mechanical properties across various tests including both tensile and three-point bending, outperforming the FGPLA counterparts. In contrast, AFPLA and FGPLA strength levels appear to be comparable when subjected to the ASTM tensile test. Notably, the strength of CFPLA demonstrates a remarkable enhancement, registering an impressive surge of 1027.5 % and 497.3 % in comparison to pure PLA in both the ASTM tensile and three-point bending tests. Although the maximum stress values for AFPLA and FGPLA remain closely aligned, a discernible distinction emerges in the context of three-point bending. It is worth noting that in tensile tests, FGPLA exhibits a greater strain at the fracture point, indicating a noteworthy mechanical behaviour.

The results from the three-point bending test unequivocally indicate that incorporating fibres into PLA material can enhance its strength, consistent with findings from prior research on PLA/Kevlar conducted by Cersoli et al. [56]. Meanwhile, this procedure concurrently reduces material usage and waste. This application holds substantial promise for real-world scenarios, particularly in the realm of 4DP, where it allows to produce of diverse items with reduced material input without compromising their mechanical properties. This development not only enhances structural robustness but also makes a notable contribution to environmentally conscious manufacturing practices.

As depicted in Fig. 4e, initial fractures emerge within the layers, progressing along the length of the specimen as the load intensifies. This leads to a separation between the two layers. When the interlayer fractures intersect, they generate perpendicular fractures in the layer directly beneath the applied load point. Simultaneously, tensile fractures form in the lowest layer beneath the neutral axis. Both types of fractures, originating from opposite sides, advance towards each other, ultimately culminating in failure. The observed failure modes in the experiments encompass delamination, matrix cracking, as well as fibre/matrix detachment and fibre rupture. It is noteworthy that delamination significantly influences the initiation of failure. Subsequently, after delamination, fibre/matrix detachment takes on a more prominent role compared to other modes of failure. The same issue occurred with the tensile test samples, as illustrated in Fig. 4f, where both the matrix and fibres experienced breakage. However, it's worth noting that some fibres remained bonded and no cracks developed in those fibres due to their robust adhesion.

For a more in-depth examination of the fibre/matrix bonding, the fracture surface of the CFRCs specimen is sectioned, and several photographs are taken using an optical microscope and SEM (see Fig. 4g and h). It is evident that the ends of the fibres are susceptible to void formation. This phenomenon may be attributed to fibre shrinkage and an uneven distribution of the molten polymer during the printing process. These images indicate that the fibre/matrix bonding persists until the final fracture, with observable fibre pull-out at the fractured section of the bending specimens. A key factor constraining the increase in fibre volume fraction is the presence of certain limitations in the printing process, such as the minimum return radius. This radius is defined as the distance that the fibre must circulate and loop around when it reaches the end of the specimen [16]. If this radius falls below a critical threshold, the fibres are pulled out from the matrix, resulting in fibre
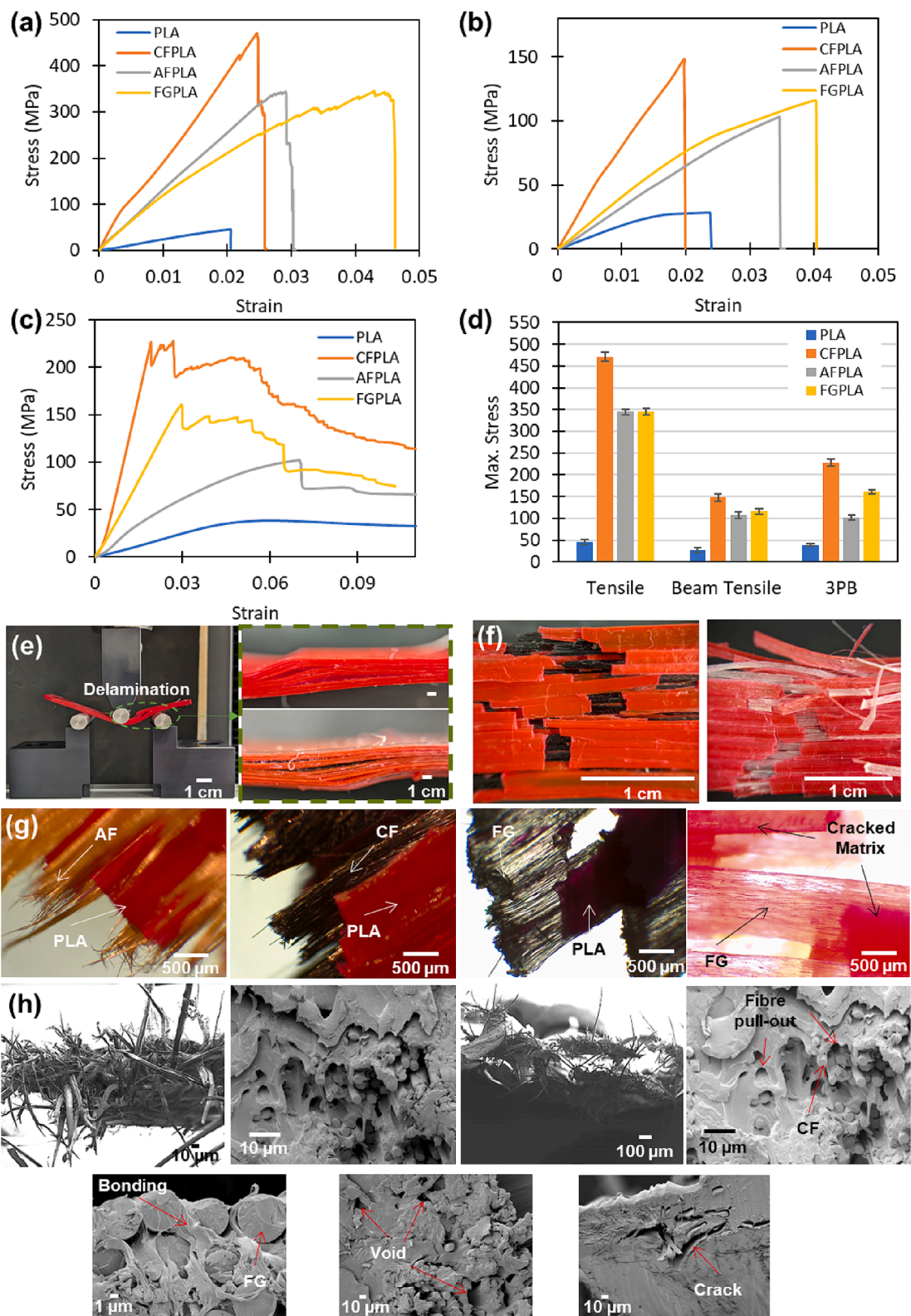
Fig. 4. Tensile test outcomes for printed samples according to (a) ASTM standards and (b) for printed CFRC beams. (c) Results of three-point bending tests for printed CFRCs and PLA. (d) Peak stress values for printed CFRCs through both tensile and three-point bending tests. (e) Evaluation of delamination in printed CFRCs through three-point bending tests. (f) Instances of partially cracked printed CFRCs, where the matrix is fractured but the fibres within the matrix remain intact. (g) Optical and (h) SEM imagery depicting areas of failure in CFRCs.

breakage. Consequently, there must inevitably be a gap between the two parallel paths of the fibres, as depicted in SEM images in Fig. 4**h**.

Furthermore, to evaluate the shape memory characteristics of CFRCs in relation to their mechanical properties, the DMA test is carried out on all printed composites under uniform size and printing conditions. Fig. 5 illustrates the storage modulus and tan δ values for both pure PLA and SMPCs. The results indicate a notable increase in the storage modulus of SMPCs compared to PLA. However, the Tan δ is lower in CFRCs compared to PLA. This is attributed to the relatively rigid nature of printed CFRCs in contrast to pure PLA. Consequently, the incorporation of fibres significantly augments the stiffness, strength, and overall mechanical attributes of the PLA matrix. The T_g of pure PLA stands at approximately 61 °C, whereas for AFPLA and FGPLA, it is around 64 °C and 70 °C for CFPLA. Furthermore, to ensure consistent results in shape memory properties, all samples are tested at temperatures surpassing their respective T_g values.

3.2. Shape memory property

In the methodology section, both cold and hot programming techniques are applied to all printed PLA and CFRC samples. The objective is to investigate how the inclusion of a layer of fibre impacts the shape fixity and recovery of SMPCs. During cold programming, the presence of fibres within the PLA matrix leads to increased rigidity of the samples. Fig. 6**a** provides an illustration of the programmed shape and the subsequent recovered shape in cold programming for FGPLA specimens. The printed samples are held in a vertical position using a gripper to evaluate their shape memory behaviour. Temperature measurements are taken using a combination of a thermocouple and an infrared camera. As observed in the cold-programmed shape of FGPLA, the FGPLA beam tends to revert to its initial shape after cold programming, a result of its higher stiffness compared to hot programming. Consequently, this has an impact on the shape fixity of printed CFRCs. By subjecting the beam to heat from a heating gun at a specific distance, the sample regains its original shape due to the SME of the PLA matrix. The same process is carried out in hot programming, as depicted in Fig. 6**b**. However, due to the nature of hot programming, the sample exhibits higher shape fixity, a point that will be further discussed later. The infrared images clearly demonstrate the return of the printed FGPLA composites to their original shape after the application of heat.

Furthermore, the study involves precise documentation of the trajectory of samples during both their programmed and recovered stages. This is accomplished through the utilization of a camera in conjunction with Capstone software, enabling a thorough assessment of their shape recovery percentage and fixity. In Fig. 6**c and d**, we visually depict the programmed and subsequently recovered shape of the FGPLA specimen

under conditions of both cold and hot programming. In addition, to ensure the robustness of our data, we meticulously monitor the temperature of each specimen using a thermocouple. This step is crucial in confirming the consistency of the experimental conditions. As demonstrated in Fig. 6**e**, the graph illustrates the temperature increase to 70 °C over time, meticulously recorded by the thermocouple wire. It is evident that the temperature progression in both cold and hot programming phases follows a comparable trend, further substantiating the reliability of our experimental setup.

The performance of SMPCs that have been printed is thoroughly assessed. In Fig. 7**a**, we can see the recorded ratios of how well the shape is maintained for beams that have undergone both cold and hot programming. When hot programming is applied, there is a significant improvement in how well the shape is retained. For instance, in CFPLA and AFPLA, the ability to maintain shape increases from 24 % to 78 % and 38 % to 92 % when transitioning from cold to hot programming, respectively. On the other hand, in cold programming, the ability to maintain shape decreases because the fibres and PLA matrix become stiffer and stronger at room temperature compared to programming at temperatures above T_g. Among these materials, pure PLA has the highest ability to maintain shape, followed by AFPLA and FGPLA in both cold and hot programming. The CFPLA printed beams exhibit the lowest ability to maintain shape. When the material is subjected to cold programming, however, it tends to lose some of its shape-holding ability due to the fibres and PLA becoming stronger and less flexible at room temperature.

Furthermore, Fig. 7**b** illustrates the shape recovery ratio of 3D-printed SMPCs. A set of 10 specimens is used for each variant. Notably, beams crafted solely from PLA exhibit the most exceptional shape recovery, boasting an impressive 97.9 % in cold and 98.3 % in hot programming. Following closely are the FGPLA composites, displaying the second-highest shape recovery rates at 95.3 % in cold and 96.1 % in hot programming. The CFPLA specimens demonstrate comparable shape recovery to the FGPLA, albeit slightly lower. This disparity arises from the inherently greater rigidity of CF as opposed to FG, particularly noticeable during cold programming, where fibre breakage may occur in CFPLA. In contrast, printed AFPLA beams exhibit the lowest shape recovery performance. The introduction of AF into PLA significantly diminishes the material's shape recovery capabilities, resulting in a stark reduction. Specifically, the shape recovery ratio for AFPLA stands at 81.2 % in cold and 83.2 % in hot conditions [30]. These findings unequivocally underscore that the incorporation of fibres leads to a reduction in the shape recovery performance of printed CFRCs.

Continuous fibres in 3D printed PLA can diminish shape recovery primarily due to their inherent structural properties. When integrated into the PLA matrix, these fibres introduce a level of rigidity and stiffness
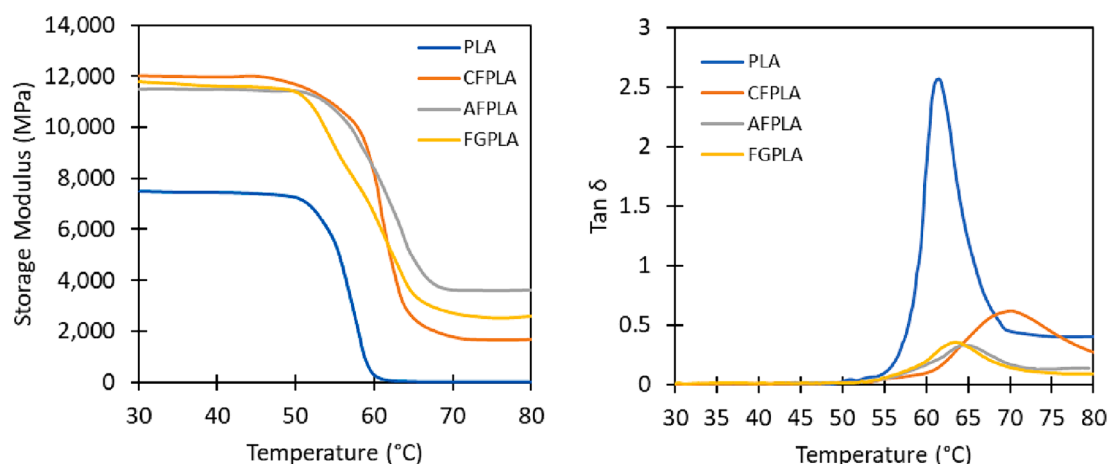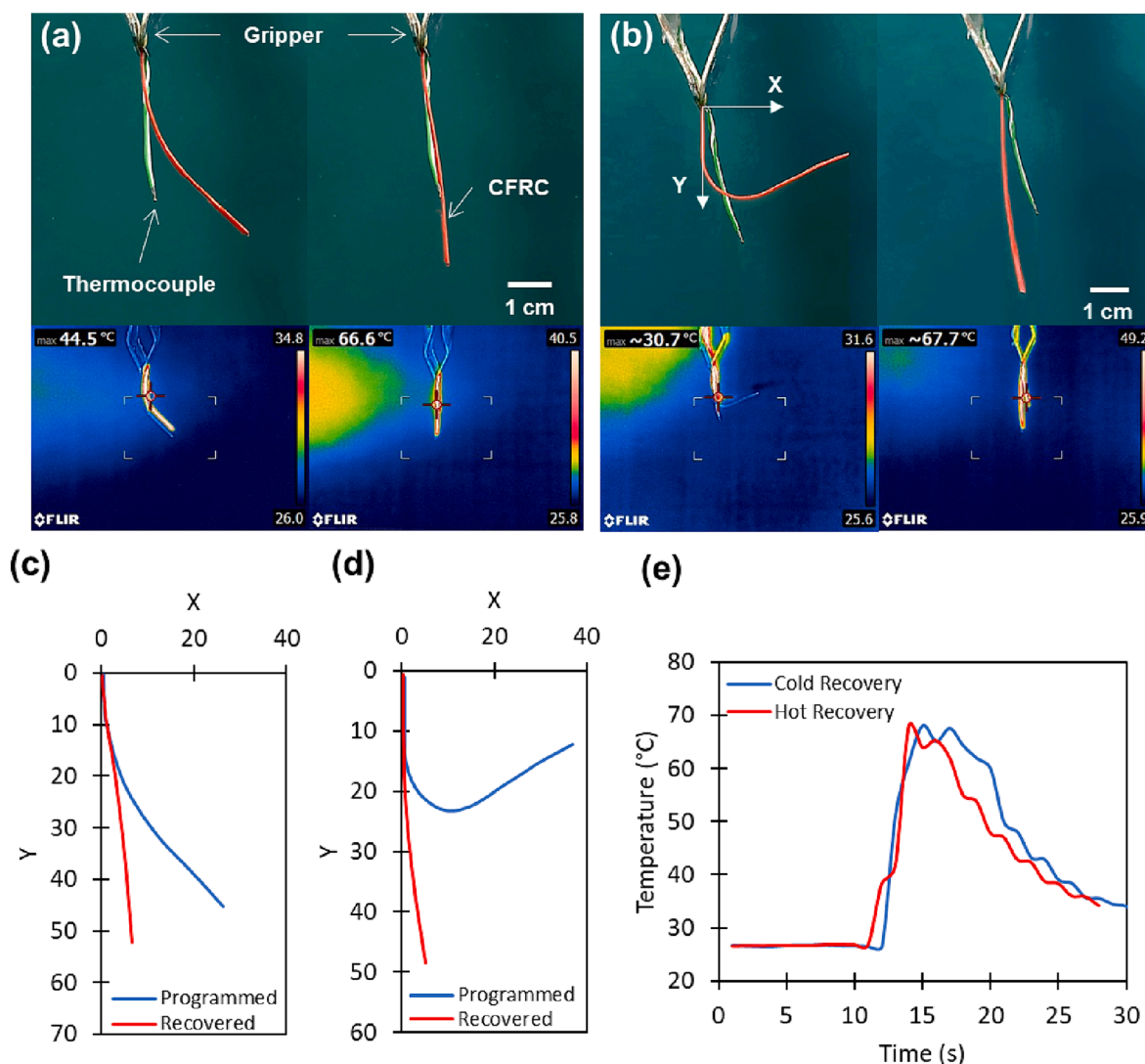

**Fig. 5.** DMA findings for printed CFRCs and PLA matrix.

Fig. 6. (a) Fixed shape and recovered shape of cold-programmed printed FGPLA beam illustrated with Infrared imagery at the initiation of heating and the conclusion of the cycle. (b) Fixed shape and recovered shape of hot-programmed printed FGPLA beam displayed with Infrared images at the initiation of heating and the conclusion of the cycle. (c) The projection of fixed and recovered shape of FGPLA beam through cold programming. (d) The projection of fixed and recovered shape of FGPLA beam through hot programming. (e) Temperature recorded over time using a thermocouple during the shape recovery process in both cold and hot programming.

that may not harmonize with the more flexible nature of the polymer [35]. This discrepancy in material behaviour can lead to a reduction in the composite's overall elasticity, hindering its ability to return to its original shape after deformation. Additionally, if the fibres are unevenly distributed or misaligned, they can create localized stress concentrations within the material, further impeding shape recovery [25]. Moreover, the bonding strength between the fibres and the PLA matrix plays a crucial role; if this interface is weak, it can result in delamination or separation, weakening the material's capacity to regain its initial form. Therefore, thoughtful consideration of factors like fibre type, orientation, concentration, and processing techniques is essential to optimize the performance of continuous fibre-reinforced 3D printed PLA composites.

Moreover, the investigation includes monitoring the shape recovery of SMPC beams after undergoing hot programming. Hot programming is preferred due to its prolonged shape recovery duration, enabling more precise time measurements. As shown in Fig. 7c, CFPLA and FGPLA composites regain their shape more rapidly compared to AFPLA and PLA [32,57]. This can be attributed to the rigid and brittle nature of the fibres in this context. Fig. 7d provides data indicating that PLA takes 8 s to

recover its shape, while CFPLA and FGPLA only require 5.5 and 6.2 s from the initiation of heating, respectively. However, AFPLA necessitates 7 s, which is a bit similar to PLA. This is due to the fact that AF exhibits a softer nature compared to CF and FG, as indicated by the results of the three-point bending test. It's worth noting that while CFRCs exhibit faster shape recovery, their shape recovery ratio is lower compared to pure PLA.

A shape recovery test involving cycles of both cold and hot programming is being carried out, as depicted in Fig. 7e and f. The test involves specimens resembling 4D-printed beams. These specimens undergo 20 cycles of alternating cold and hot programming followed by recovery. In both the cold and hot programming phases, pure PLA consistently exhibits shape recovery, fully returning to its original form [58]. However, for CFRCs, there is a slight reduction in the shape recovery ratio, particularly noticeable during cold programming. In contrast, FGPLA demonstrates superior performance in the cyclic test during the hot programming phase when compared to CFPLA and AFPLA. This suggests that SMPCs perform better in hot programming conditions compared to cold programming due to their reduced stiffness during the shape programming process. Additionally, the brittleness of
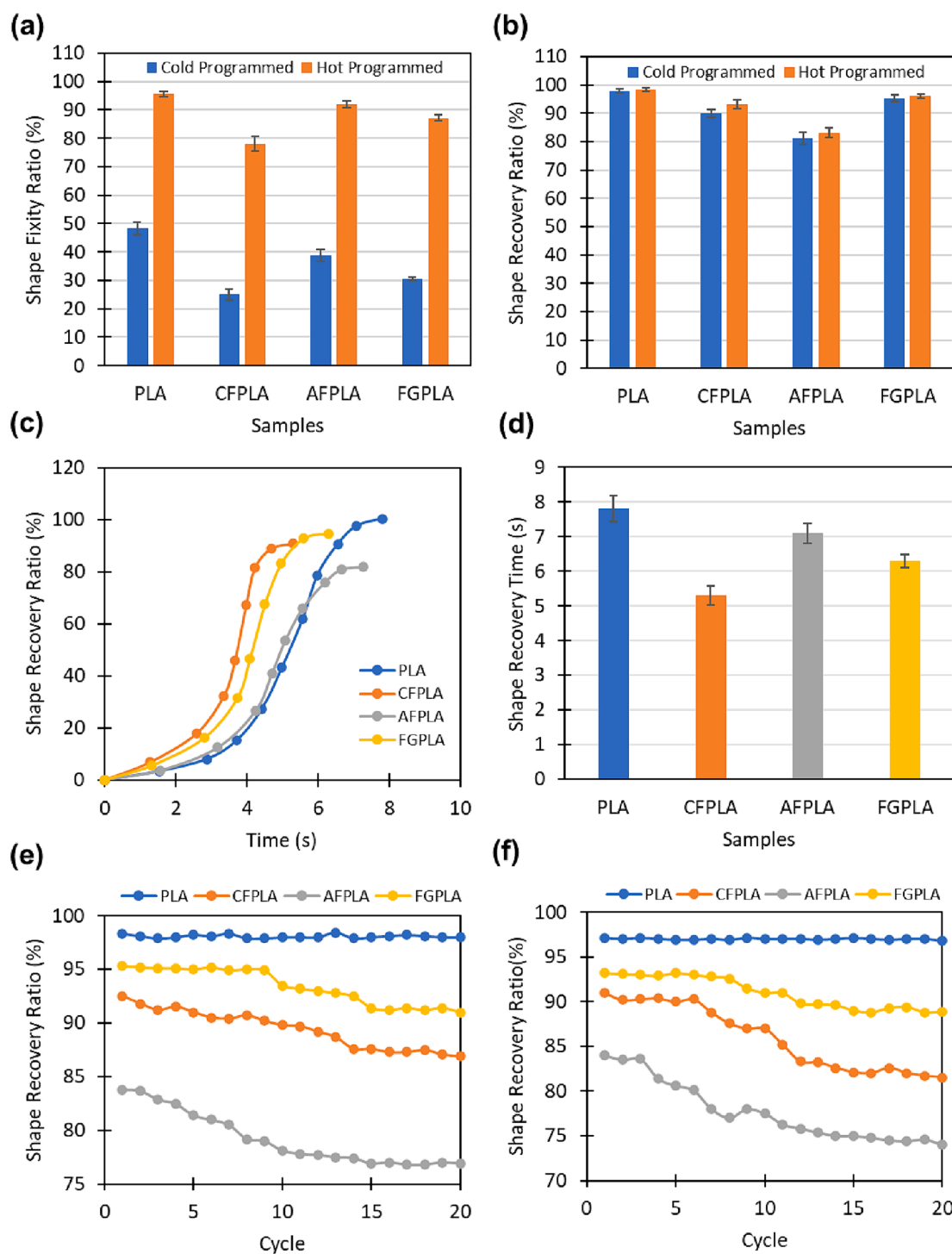
Fig. 7. (a) Shape fixity ratio for printed SMPCs and PLA using cold/hot programming. (b) Shape recovery ratio for printed CFRCs and PLA using cold/hot programming. (c) Evolution of shape recovery ratio over time for printed SMPCs and PLA in hot programming. (d) A contrast between the shape recovery time of SMPCs and PLA. (e) Cyclic shape recovery ratio in cold programming. (f) Cyclic shape recovery ratio in hot programming.

both PLA and fibres is less during hot programming, resulting in an increase in shape fixity.

In short, FGPLA outperforms AFPLA and CFPLA in terms of both shape recovery and cyclic shape recovery after PLA samples. It's important to highlight that the cyclic shape recovery of CFRCs can see improvement if the applied programming load is reduced to 20 %. While CFPLA shares similar shape recovery characteristics, FGPLA demonstrates more consistent performance in cyclic shape properties. Additionally, FGPLA exhibits the second-highest mechanical strength,

trailing only behind CFPLA in both tensile and three-point bending tests. This is attributed to the superior bonding between PLA and FG during printing, as well as FG's reduced brittleness compared to CF. Notably, CF's higher stiffness creates a mismatch with the PLA matrix, leading to diminished performance in cyclic shape memory tests for CFPLA. Consequently, FG is the preferred choice for applications due to these mentioned advantages over other fibres.

4. Applications

4.1. Human-Material interaction

Recently, there has been a sustained fascination and focus on 4DP within the realm of human-material interaction [22,59]. The importance of design principles that support the creation of environmentally sustainable 4D-printed items is underscored, with a focus on minimizing material usage and waste. Custom and personalised products that are perfectly suited to a certain product's requirements may be produced thanks to FFF 4DP technology. This versatility makes it possible to create unique gadgets that closely match user preferences, resulting in an improved user experience and more satisfaction [60]. Furthermore, FFF 4DP offers a cost-effective manufacturing solution through product reusability, eliminating the need for complex tooling and moulds commonly associated with traditional manufacturing methods [4]. The availability and user-friendly characteristics of non-toxic materials in FFF 4DP enhance the overall appropriateness and usefulness of 4D-printed devices produced using this technology [61].

In this work, several designs are developed focusing on human-material interaction. These designs are notable for their reusability, lightweight construction, and durability, all attributed to the incorporation of continuous FG within a PLA matrix. Fig. 8a showcases the initial design, specifically the beam actuator with specified dimensions. This hook-shaped actuator weighs 0.36 g and, following hot programming of its shape demonstrates the ability to securely hold a key or lift and hold objects weighing up to 500 g. Remarkably, the beam actuator can support a dead load equivalent to 1385 times its weight. In contrast, when tested under similar conditions, the beam PLA matrix alone breaks under the heavy load. Additionally, this actuator holder boasts a remarkable shape recovery ratio of 94 % after heating, making it suitable for reuse in various consumer products as needed. This feature not only minimizes material consumption and waste but also contributes to a more sustainable design approach.

Meanwhile, an alternative configuration is conceived, presented as a locker in Fig. 8b. This actuator locker weighs 0.94 g and exhibits an impressive shape recovery rate of 96 %. The degree of shape recovery in printed SMPC products hinges on factors such as design and product thickness. The process encompassing shape programming, shape locking, and shape recovery of these actuators is examined accordingly. One shape-programmed arrangement of the design is established, yet there exists the potential to adapt and amend the shape programming as needed. By incorporating continuous FG, the actuator design can be adjusted to function as a robust locker, endowed with high strength. This design can secure its shape onto an object, subsequently grasping and securing another object on the opposite side of the actuator.

Another human-material interaction design is related to the field of the field of orthopaedics [62]. A plastic finger splint is a multipurpose, portable medical aid used to brace and immobilise broken or damaged fingers [63]. Plastic finger splints are a vital tool in the treatment of finger injuries because of how simple they are to apply and how well they work to speed rehabilitation, allowing patients to regain functioning. A 2-D sheet is employed to craft a sustainable CFRC finger splint tailored for a patient. In Fig. 8c, the initial design of the splint, the process of hot shaping, the subsequent shape recovery, and the ultimate regained form are shown. This lightweight splint (2.79 g) demonstrates an impressive shape recovery rate of about 95 %, and its design permits multiple reuses. Notably, no top layer matrix cover is used in its fabrication to investigate how the fibres behave post the shaping and recovery stages. As shown in Fig. 8c, some fibre fragmentation does occur in the bent area after shape recovery. However, due to the inherent properties of the fibres and the strong bond between PLA and FG, this does not compromise the splint's ability to be reused or its mechanical strength. The splint is constructed from plastic with continuous fibres and is meticulously shaped to snugly fit over the injured finger, providing support for both the finger joints and palm. Its adjustability

ensures a secure fit for a range of finger sizes smaller than the one depicted in Fig. 8c. Furthermore, these plastic finger splints are often translucent, allowing for easy monitoring of the wounded area, which can be crucial in assessing the progress of healing. Meanwhile, another advantage of this method is using other types of thermoplastics by modifying the printing settings. In brief, these concepts apply to materials exhibiting SME. However, establishing a robust connection between continuous fibres and the matrix poses a notable challenge. While exploring diverse materials for advancing this application is plausible, it's crucial to emphasize that alternative materials must possess SME to restore their form for reuse, a pivotal feature found in finger splints but often absent in the majority of materials utilized in the FFF process. Moreover, attaining a robust bond between continuous fibre and matrix introduces another considerable hurdle, particularly when modifying the matrix composition.

The manufacture of SMPC consumer goods contributes to a reduction in material usage without compromising strength in the realm of human-material interaction. The outstanding strength-to-weight ratio of CFRCs makes them the perfect choice for a variety of applications. Contrary to traditional materials like metals or solid plastics, SMPCs enable the production of durable items with a substantially lower material usage. This is accomplished by utilising the inherent strength of continuous fibres. In today's ecologically concerned climate, when resource conservation is of the highest significance, this reduction in material utilisation is crucial. Additionally, the shape recovery capabilities of printed SMPCs enable product reusability, leading to a decrease in material waste. Another benefit of 4D-printed SMPCs pertains to packaging. Given the nature of 2D sheet printing involved in this process, it becomes feasible to transport products with compact and minimized packaging. Consequently, this aids in cost reduction for both packaging and delivery. This not only simplifies logistics but also lessens the environmental effect of the packing and shipping processes.

4.2. Cellular meta-composite structures

There are several intrinsic benefits of lattice or cellular structures, including their lightweight, excellent specific strength, and stiffness [64]. Due to these qualities, lattices are being thoroughly researched in various fields [65]. Incorporating a hierarchical arrangement into lattice structures shows its capacity to withstand heavy loads. These specialised lattice structures have been successfully used in a variety of building sectors because of their minimal weight and amazing strength [66]. A few examples of materials having a reputation for being lightweight are honeycomb structures, which have been the focus of extensive research and development due to the wide range of applications they have [67–70]. To evaluate the effectiveness of cold programming and shape recovery in CFRCs, a 2D honeycomb cellular structure is created. The compression phases and cyclic loading graphs for this construction are shown in Fig. 9. In each compression test, three specimens are used, employing a 50 kN load cell at a speed of 2 mm/min. The structure undergoes cyclic compression up to 80 % of the initial height which is 62 mm, as depicted in Fig. 9a. Subsequently, the structure is completely unloaded, as illustrated in the image. An identical procedure is applied to another specimen, this time up to 50 % strain, to discern the impact of minimal loading on the honeycomb structure (see Fig. 9b). The structures are then heated past their T_g to regain their original shape and return to their initial height. The shape recovery ratio in this test is determined by the ratio of the recovered height to the initial height.

The outcomes of the cyclic compression test following heating and shape recovery are meticulously observed and recorded. Fig. 9c and d present the findings of the cyclic compression tests, conducted up to 80 % and 50 % strain, respectively. Additionally, Fig. 9e displays the results of shape recovery for structures subjected to cyclic thermo-mechanical loading. Based on the acquired data, it is evident that when the structure is loaded up to 80 % strain, its shape recovery drops to 92 %. Consequently, the structure's performance is compromised, as
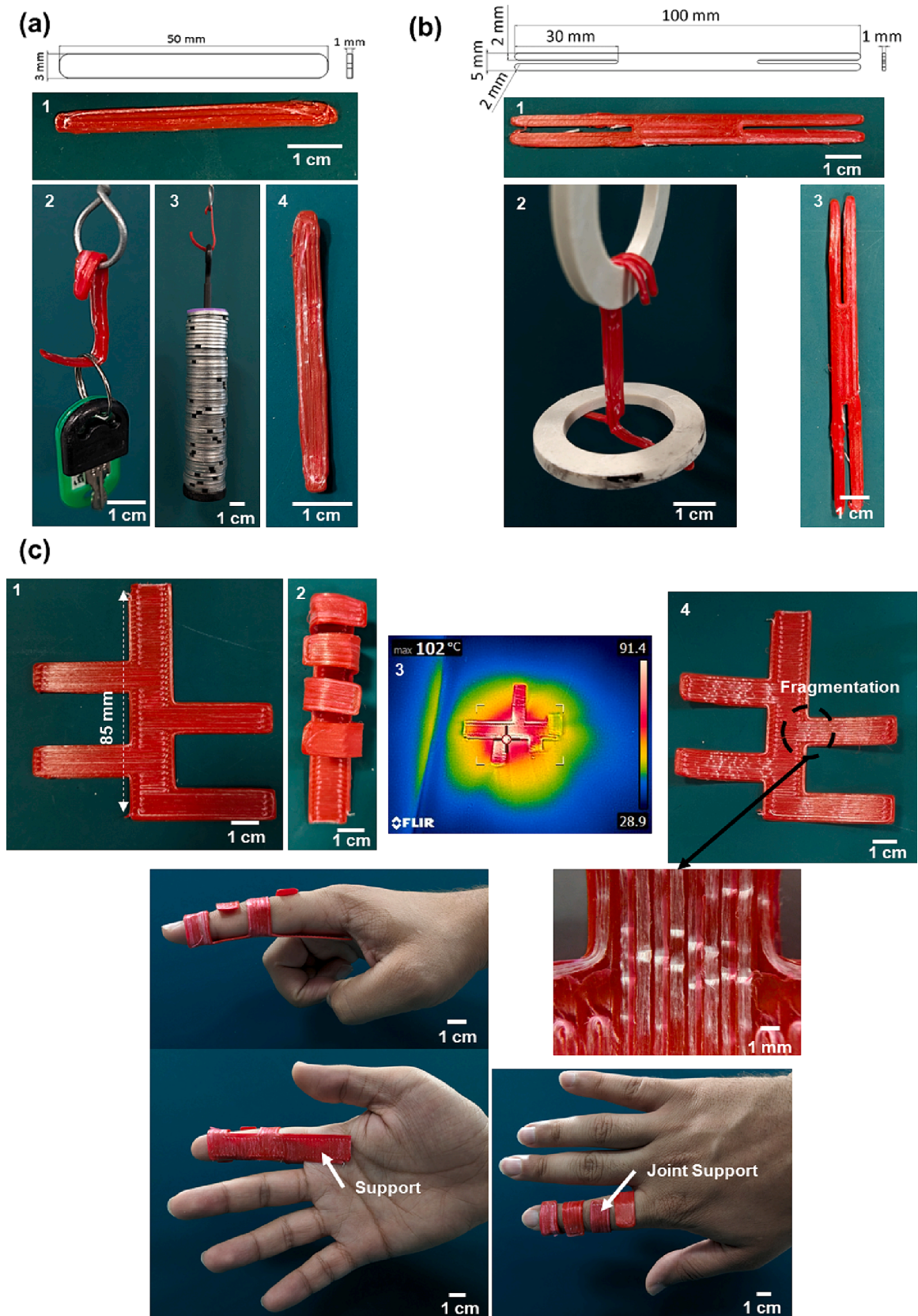
Fig. 8. (a) Images depicting the printed SMPC actuator holder, along with stages of hot shape programming, applications, and shape recovery shown in 1 through 4. (b) Images illustrating the printed locker, as well as the steps of shape programming and recovery outlined from 1 to 3. (c) 1. Image of the printed SMPC finger splint. 2. Programmed CFRC splint. 3. Infrared image captured during the shape recovery process. 4. Final shape of the recovered finger splint with observed fragmentation in FG fibres. The finger splint is designed to provide support for the pointed finger joint.
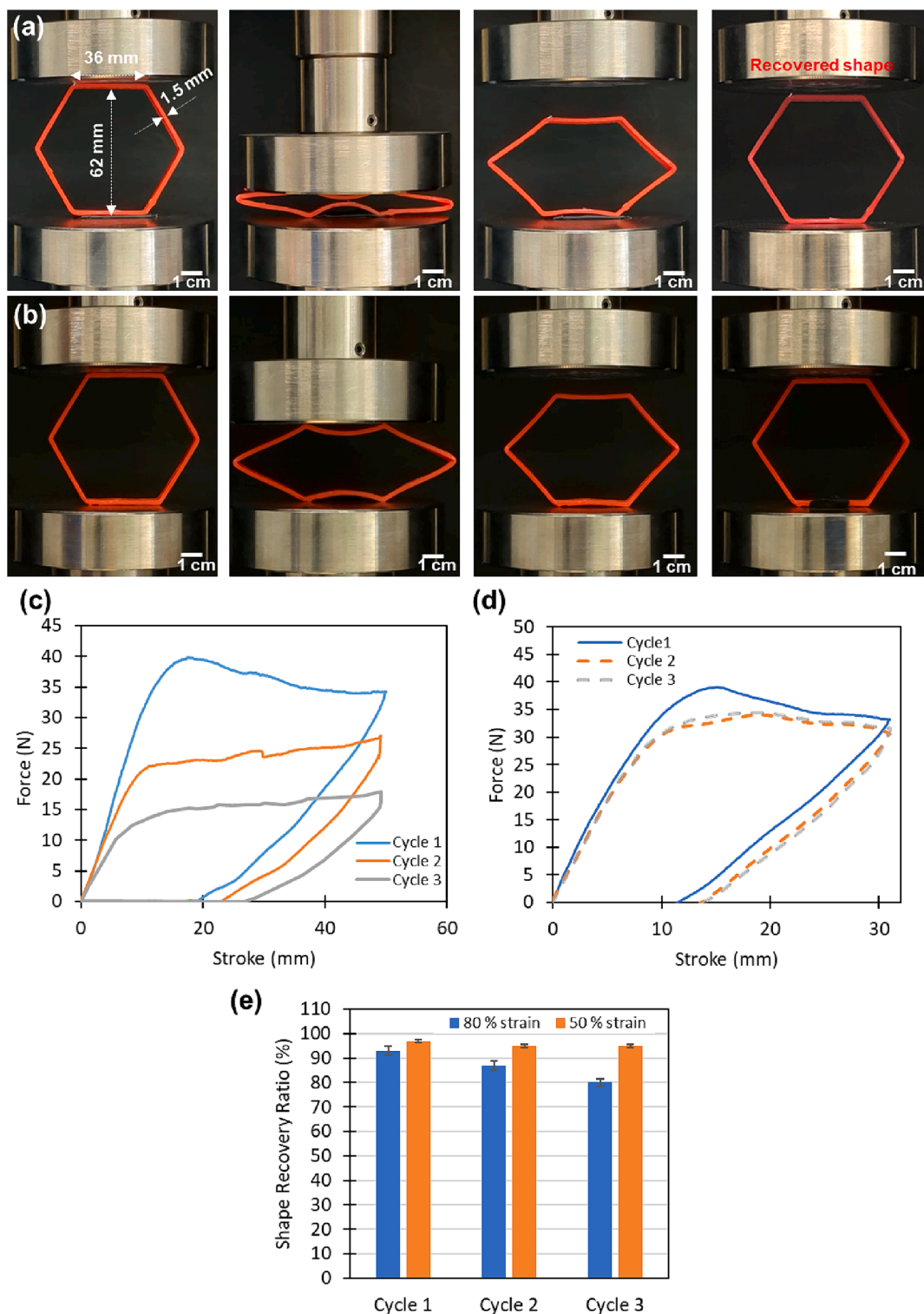
Fig. 9. (a) Progression of the compression test and loading/unloading process for CFRC honeycomb up to 80% strain. (b) The sequence of stages during the compression test and loading/unloading of SMPC honeycomb up to 50% strain. (c) Results of force versus stroke during cyclic loading on a single sample after shape recovery through heating up to 80% strain. (d) Results of force versus stroke during cyclic loading on a single sample after shape recovery through heating up to 50% strain. (e) The shape recovery ratio of printed SMPC honeycomb after unloading in cyclic compression tests.

it fails to completely regain its original shape. This is attributed to the extensive displacement experienced during loading, leading to plastic deformation of the sample and internal cracks in the PLA matrix. Moreover, as illustrated in Fig. 9c, after each cycle, the structure's performance and shape recovery continue to deteriorate. In contrast, when the structure is compressed up to 50 % strain, the shape recovery

after heating reaches approximately 96 %. This notable recovery is attributed to the incorporation of continuous fibres in the meta-composite structure. The compression test and subsequent shape recovery results indicate that after the loading and unloading, the outcomes remain consistent in cycles 2 and 3. This suggests that the structure can be reused effectively, thanks to its high shape recovery

properties and improved performance.

Moreover, the constructed structures have the ability to absorb a substantial amount of energy during compression without putting themselves under excessive stress [71,72]. They are capable of significant compressive deformation at a particular stress threshold, making this conceivable. The basic idea behind energy absorption in meta-composite structures is that they may change the kinetic energy from an impact into different types of energy through processes including elastic or plastic deformation, mechanical instabilities, and fracture. Fig. 10a shows the dissipated energy and absorbed energy from the force–displacement graph. Energy absorption (EA) and specific energy absorption (SEA) are investigated for the structures as well. The EA and SEA are calculated as follows:

$$EA = \int_0^d F_{(x)} d_x \tag{5}$$

$$SEA = \frac{EA}{m} \tag{6}$$

The EA can be calculated by finding the area beneath the load–displacement curve. F(x) represents the displacement function, while d signifies the deformation. The overall energy absorption refers to the cumulative load–displacement graph spanning from zero to the highest deformation point. SEA is determined by the energy absorption value per unit mass. Fig. 10b displays the outcomes of SEA for cellular SMPC specimens. For samples with 80 % compression, SEA values exhibit a steep decline after the initial cycle. Conversely, samples subjected to compression up to 50 % strain undergo a relatively modest decrease, yielding values of 0.055 for SEA. In both structures examined in this study, the amount of energy dissipated exceeds that which is absorbed. This is attributed to the plastic hardening characteristics of both the PLA material and the lattice structure, resulting in more energy being dissipated rather than absorbed. Nonetheless, the design demonstrates consistent effectiveness in its capacity for reuse.

Cellular structures find extensive use in industries like automobiles, marine, and aerospace, owing to their favourable attributes like lightweight construction and impressive energy absorption potential. In practical applications, both the energy absorption capacity and the weight of the sandwich structure hold significant importance. Therefore, by augmenting the number of unit cells, it becomes feasible to create SMP meta-composite structures with significant applications across diverse fields, thanks to their combination of high strength and low weight. The resultant materials have the potential to push the limits of strength-to-weight ratios, creating new possibilities for use in the construction, automotive, aerospace, and other industries. The future promises the potential of safer, more effective, and ecologically sustainable solutions across a variety of sectors as we stand on the edge of

this transformational breakthrough.

5. Conclusion

This research employed FFF technology to perform 4DP of CFRCs utilizing various fibre types through cold and hot programming techniques. The objective was to employ continuous fibres to minimize material usage and decrease the weight of plastic for 4D-printed products. This approach contributes to sustainability due to its reusability and promotes eco-friendly design principles. An FFF 3D printer with one feed channel was modified to manufacture CFRCs with different continuous fibres. Various types of fibres, such as CF, FG, and AF, were simultaneously printed with a PLA matrix using a specialized nozzle. Consistent printing parameters were applied for both pure PLA and CFRCs. Three-point bending and tensile experiments were carried out to evaluate the impact of different fibres on the tensile and bending strength of 4D-printed SMPCs. The findings indicate that CFPLA exhibits superior tensile and bending performance in terms of mechanical properties, followed by FGPLA and AFPLA, with all three significantly outperforming pure PLA. The tensile and bending properties of CFPLA exhibited a remarkable increase, reaching up to 1027.5 % and 497.3 % respectively, compared to pure PLA. The variable stiffness property and SME of the 4D-printed CFRCs were evaluated using DMA and heating form recovery tests, respectively.

Despite the substantial enhancement in mechanical properties, the shape memory attributes of CFRCs were found to be inferior to those of pure PLA. Specifically, the shape recovery ratio for basic CFRC beams was approximately 93.2 % for CFPLA, 95.6 % for FGPLA, and 83 % for AFPLA, whereas it reached almost 100 % for pure PLA. Nevertheless, the shape recovery time was quicker for CFRCs owing to their higher stiffness and strength. Moreover, cyclic shape tests were conducted for 20 cycles, and after a few cycles, the shape recovery ratio of CFRCs experienced a slight decline, with FGPLA demonstrating the best performance in the cyclic test. Notably, among the fibres, FG exhibited the most favourable performance due to its reliable and superior shape recovery ratio, as well as commendable mechanical properties when combined with CFPLA. FGPLA was employed to demonstrate the practical application of 4D-printed SMPCs. Human-material interaction and cellular structures were selected to assess the performance of printed FGPLA in real-world scenarios. Items such as a hook-shaped holder, locker, and finger splint were 4D-printed as consumer products, designed with reusability features. For example, the 4D-printed hook/holder, weighing 0.36 g, demonstrated the capability to support loads of up to 500 g. Additionally, a single cell of a cellular meta-composite structure was printed to evaluate its performance in cyclic compression loading, cold programming, and subsequent shape recovery.

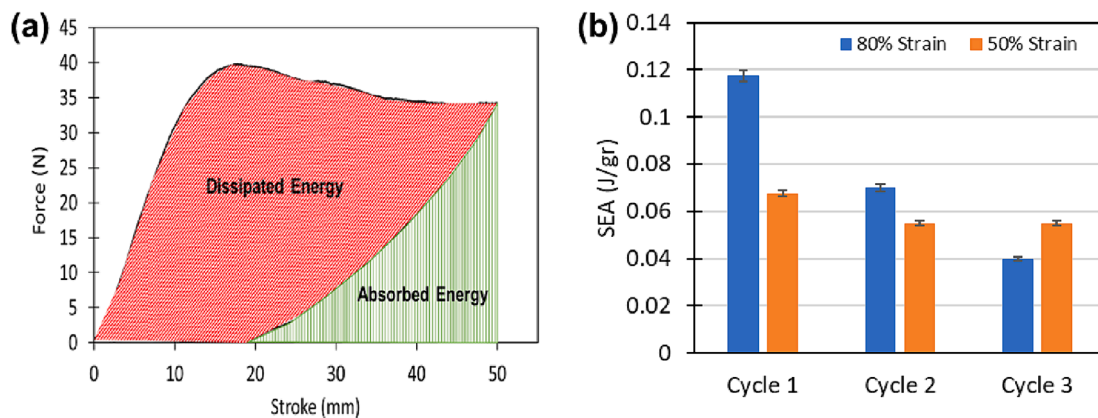In conclusion, compared to typical 3D-printed pure polymer or

Fig. 10. (a) Distribution of absorbed and dissipated energy from the first cycle up to 80% strain. (b) SEA observed in cyclic compression tests at 50% and 80% strain levels.

particle-reinforced composite structures, the CFRCs significantly increase mechanical strength. It also addresses the limitations of conventional 3D-printed structures, which lack active deformation capabilities. Therefore, it plays a pivotal role in sustainable design by significantly reducing material consumption and waste in consumer products. CFRCs produced via 4DP offer a unique manufacturing strategy, and to further expand the technology's potential applications, future work should focus on creating complicated components.

CRediT authorship contribution statement

Mohammadreza Lalegani Dezaki: Writing – original draft, Validation, Methodology, Investigation, Formal analysis, Conceptualization. **Mahdi Bodaghi:** Writing – review & editing, Supervision, Resources, Project administration, Methodology, Investigation, Funding acquisition, Formal analysis, Conceptualization.

Declaration of competing interest

The authors declare that they have no known competing financial interests or personal relationships that could have appeared to influence the work reported in this paper.

Data availability

Data will be made available on request.

Acknowledgements

References

[1] M.Y. Khalid, Z.U. Arif, R. Noroozi, A. Zolfagharian, M. Bodaghi, 4D printing of shape memory polymer composites: a review on fabrication techniques, applications, and future perspectives, J. Manuf. Process. 81 (2022) 759–797, https://doi.org/10.1016/j.jmapro.2022.07.035.

[2] L.P. Muthe, K. Pickering, C. Gauss, A review of 3D/4D printing of poly-lactic acid composites with bio-derived reinforcements, Compo. Part C, Open Access 8 (2022) 100271, https://doi.org/10.1016/j.jcomc.2022.100271.

[3] W. Wei, J. Liu, J. Huang, F. Cao, K. Qian, Y. Yao, W. Li, Recent advances and perspectives of shape memory polymer fibers, Eur. Polym. J. 175 (2022) 111385, https://doi.org/10.1016/j.eurpolymj.2022.111385.

[4] M. Lalegani Dezaki, M. Bodaghi, Sustainable 4D printing of magneto-electroactive shape memory polymer composites, Int. J. Adv. Manuf. Technol. 126 (1–2) (2023) 35–48, https://doi.org/10.1007/s00170-023-11101-0.

[5] W. Zhao, N. Li, L. Liu, J. Leng, Y. Liu, Mechanical behaviors and applications of shape memory polymer and its composites, Appl. Physics Reviews 10 (1) (2023), https://doi.org/10.1063/5.0126892.

[6] Y. Xia, Y. He, F. Zhang, Y. Liu, J. Leng, A review of shape memory polymers and composites: mechanisms, materials, and applications, Adv. Mater. (Weinheim) 33 (6) (2021), https://doi.org/10.1002/adma.202000713.

[7] M. Lalegani Dezaki, M. Bodaghi, A review of recent manufacturing technologies for sustainable soft actuators, Int. J. Precision Engineering and Manufacturing-Green Technol. (2023), https://doi.org/10.1007/s40684-023-00533-4.

[8] H. Soleimanzadeh, B. Rolfe, M. Bodaghi, M. Jamalabadi, X. Zhang, A. Zolfagharian, Sustainable robots 4D printing, Adv Sustainable Syst (2023), https://doi.org/10.1002/adsu.202300289.

[9] J. Carrell, G. Gruss, E. Gomez, Four-dimensional printing using fused-deposition modeling: a review, Rapid Prototyp. J. 26 (5) (2020) 855–869, https://doi.org/10.1108/RPJ-12-2018-0305.

[10] M. Mehrpouya, H. Vahabi, S. Janbaz, A. Darafsheh, T.R. Mazur, S. Ramakrishna, 4D printing of shape memory polylactic acid (PLA), Polymer (guilford) 230 (2021) 124080, https://doi.org/10.1016/j.polymer.2021.124080.

[11] M. Lalegani Dezaki, M.K.A. Mohd Ariffin, S. Hatami, An overview of fused deposition modelling (FDM): research, development and process optimisation, Rapid Prototyp. J. 27 (3) (2021) 562–582, https://doi.org/10.1108/RPJ-08-2019-0230.

[12] J.P. Rett, Y.L. Traore, E.A. Ho, Sustainable materials for fused deposition modeling 3D printing applications, Adv. Eng. Mater. 23 (7) (2021), https://doi.org/10.1002/adem.202001472.

[13] M. Lalegani Dezaki, M. Bodaghi, Shape memory meta-laminar jamming actuators fabricated by 4D printing, Soft Matter 19 (12) (2023) 2186–2223, https://doi.org/10.1039/d3sm00106g.

[14] J. Zhang, Z. Yin, L. Ren, Q. Liu, L. Ren, X. Yang, X. Zhou, Advances in 4D printed shape memory polymers: from 3D printing, smart excitation, and response to applications, Adv. Mater. Technol. 7 (9) (2022), https://doi.org/10.1002/admt.202101568.

[15] S. Liu, Y. Li, N. Li, A novel free-hanging 3D printing method for continuous carbon fiber reinforced thermoplastic lattice truss core structures, Mater. Des. 137 (2018) 235–244, https://doi.org/10.1016/j.matdes.2017.10.007.

[16] M. Heidari-Rarani, M. Rafiee-Afarani, A.M. Zahedi, Mechanical characterization of FDM 3D printing of continuous carbon fiber reinforced PLA composites, Compo. Part B, Eng. 175 (2019) 107147, https://doi.org/10.1016/j.compositesb.2019.107147.

[17] S.M.F. Kabir, K. Mathur, A.M. Seyam, A critical review on 3D printed continuous fiber-reinforced composites: history, mechanism, materials and properties, Compos. Struct. 232 (2020) 111476, https://doi.org/10.1016/j.compstruct.2019.111476.

[18] P. Parandoush, D. Lin, A review on additive manufacturing of polymer-fiber composites, Compos. Struct. 182 (2017) 36–53, https://doi.org/10.1016/j.compstruct.2017.08.088.

[19] G. Liu, Y. Xiong, L. Zhou, Additive manufacturing of continuous fiber reinforced polymer composites: design opportunities and novel applications, Compos. Commun. 27 (2021) 100907, https://doi.org/10.1016/j.coco.2021.100907.

[20] C. de Kergariou, A. Le Duigou, A. Perriman, F. Scarpa, Design space and manufacturing of programmable 4D printed continuous flax fibre polylactic acid composite hygromorphs, Mater. Des. 225 (2023) 111472, https://doi.org/10.1016/j.matdes.2022.111472.

[21] C. Zeng, L. Liu, W. Bian, J. Leng, Y. Liu, Compression behavior and energy absorption of 3D printed continuous fiber reinforced composite honeycomb structures with shape memory effects, Addit. Manuf. 38 (2021) 101842, https://doi.org/10.1016/j.addma.2021.101842.

[22] Y. Yu, H. Liu, K. Qian, H. Yang, M. McGehee, J. Gu, D. Luo, L. Yao, Y.J. Zhang, Material characterization and precise finite element analysis of fiber reinforced thermoplastic composites for 4D printing, Comp. Aided Design 122 (2020) 102817, https://doi.org/10.1016/j.cad.2020.102817.

[23] M. Rafiee, R.D. Farahani, D. Therriault, Multi-material 3D and 4D printing: a survey, Adv. Sci. 7 (12) (2020) 1902307, https://doi.org/10.1002/advs.201902307.

[24] H. Wang, Z. Zhang, K. Fu, Y. Li, Four-dimensionally printed continuous carbon fiber-reinforced shape memory polymer composites with diverse deformation based on an inhomogeneous temperature field, Polymers 15 (18) (2023) 3740, https://doi.org/10.3390/polym15183740.

[25] C. Zeng, L. Liu, W. Bian, J. Leng, Y. Liu, Temperature-dependent mechanical response of 4D printed composite lattice structures reinforced by continuous fiber, Compos. Struct. 280 (2022) 114952, https://doi.org/10.1016/j.compstruct.2021.114952.

[26] Y. Zhang, J. Qiao, G. Zhang, Y. Li, L. Li, Prediction of deformation and failure behavior of continuous fiber reinforced composite fabricated by additive manufacturing, Compos. Struct. 265 (2021) 113738, https://doi.org/10.1016/j.compstruct.2021.113738.

[27] Y. Cheng, J. Li, X. Qian, S. Rudykh, 3D printed recoverable honeycomb composites reinforced by continuous carbon fibers, Compos. Struct. 268 (2021) 113974, https://doi.org/10.1016/j.compstruct.2021.113974.

[28] C. Zeng, L. Liu, W. Bian, Y. Liu, J. Leng, 4D printed electro-induced continuous carbon fiber reinforced shape memory polymer composites with excellent bending resistance, Compos. B Eng. 194 (2020) 108034, https://doi.org/10.1016/j.compositesb.2020.108034.

[29] C. Zeng, L. Liu, W. Bian, J. Leng, Y. Liu, Bending performance and failure behavior of 3D printed continuous fiber reinforced composite corrugated sandwich structures with shape memory capability, Compos. Struct. 262 (2021) 113626, https://doi.org/10.1016/j.compstruct.2021.113626.

[30] K. Dong, H. Ke, M. Panahi-Sarmad, T. Yang, X. Huang, X. Xiao, Mechanical properties and shape memory effect of 4D printed cellular structure composite with a novel continuous fiber-reinforced printing path, Mater. Des. 198 (2021) 109303, https://doi.org/10.1016/j.matdes.2020.109303.

[31] Y. Zhou, Y. Yang, A. Jian, T. Zhou, G. Tao, L. Ren, J. Zang, Z. Zhang, Co-extrusion 4D printing of shape memory polymers with continuous metallic fibers for selective deformation, Compos. Sci. Technol. 227 (2022) 109603, https://doi.org/10.1016/j.compscitech.2022.109603.

[32] H. Chen, F. Zhang, Y. Sun, B. Sun, B. Gu, J. Leng, W. Zhang, Electrothermal shape memory behavior and recovery force of four-dimensional printed continuous carbon fiber/polylactic acid composite, SMS. 30 (2) (2021) 25040, https://doi.org/10.1088/1361-665X/abd912.

[33] C. Yang, B. Wang, D. Li, X. Tian, Modelling and characterisation for the responsive performance of CF/PLA and CF/PEEK smart materials fabricated by 4D printing, Virtual and Physical Prototyping 12 (1) (2017) 69–76, https://doi.org/10.1080/17452759.2016.1265992.

[34] M.D.H. Beg, K.L. Pickering, C. Gauss, The effects of alkaline digestion, bleaching and ultrasonication treatment of fibre on 3D printed harakeke fibre reinforced polylactic acid composites, Compo. Part A Appl. sci. manufacturing 166 (2023), https://doi.org/10.1016/j.compositesa.2022.107384.

[35] K. Dong, Y. Wang, Z. Wang, W. Qiu, P. Zheng, Y. Xiong, Reusability and energy absorption behavior of 4D printed continuous fiber-reinforced auxetic composite structures, Compos. A Appl. Sci. Manuf. 169 (2023) 107529, https://doi.org/10.1016/j.compositesa.2023.107529.

[36] Q. Wang, X. Tian, L. Huang, D. Li, A.V. Malakhov, A.N. Polilov, Programmable morphing composites with embedded continuous fibers by 4D printing, Mater. Des. 155 (2018) 404–413, https://doi.org/10.1016/j.matdes.2018.06.027.

[37] J. Xu, J. Song, 10 - Polylactic acid (PLA)-based shape-memory materials for biomedical applications, Shape Memory Polymers for Biomedical Applications (2015) 197–217, https://doi.org/10.1016/B978-0-85709-698-2.00010-6.

[38] W.B. Han, S.M. Yang, K. Rajaram, S. Hwang, Materials and fabrication strategies for biocompatible and biodegradable conductive Polymer composites toward bio-integrated electronic systems, Adv. Sustainable Syst. 6 (2) (2022) 2100075, https://doi.org/10.1002/adsu.202100075.

[39] C.H. Lee, F.N.B.M. Padzil, S.H. Lee, Z.M.A. Ainun, L.C. Abdullah, Potential for natural fiber reinforcement in PLA polymer filaments for fused deposition modeling (FDM) additive manufacturing: a review, Polymers 13 (9) (2021) 1407, https://doi.org/10.3390/polym13091407.

[40] Markforged. Fibreglass. https://markforged.com/materials/continuous-fibers/fiberglass.

[41] Markforged. Aramid Fibre (Kevlar®). https://markforged.com/materials/continuous-fibers/kevlar.

[42] Markforged. Carbon Fibre. https://markforged.com/materials/continuous-fibers/continuous-carbon-fiber.

[43] R. Matsuzaki, M. Ueda, M. Namiki, T. Jeong, H. Asahara, K. Horiguchi, T. Nakamura, A. Todoroki, Y. Hirano, Three-dimensional printing of continuous-fiber composites by in-nozzle impregnation, Sci. Rep. 6 (1) (2016) 23058, https://doi.org/10.1038/srep23058.

[44] M. Khosroupour Arabi, N. Kordani, 3D-printing of continuous fiber: a review of processes, materials and properties, Polymer-Plastics Technol. Mater. 62 (12) (2023) 1525–1559, https://doi.org/10.1080/25740881.2023.2222793.

[45] K. Chen, L. Yu, Y. Cui, M. Jia, K. Pan, Optimization of printing parameters of 3D-printed continuous glass fiber reinforced polylactic acid composites, Thin-Walled Struct. 164 (2021) 107717, https://doi.org/10.1016/j.tws.2021.107717.

[46] A. Le Duigou, A. Barbé, E. Guillou, M. Castro, 3D printing of continuous flax fibre reinforced biocomposites for structural applications, Mater. Des. 180 (2019), https://doi.org/10.1016/j.matdes.2019.107884.

[47] ASTM International. ASTM D3039. Standard Test Method for Tensile Properties of Polymer Matrix Composite Materials. 10.1520/D3039_D3039M-08.

[48] ASTM International. ASTM D638-14. Standard Test Method for Tensile Properties of Plastics. 10.1520/D0638-14.

[49] ASTM International. ASTM D790. Standard Test Methods for Flexural Properties of Unreinforced and Reinforced Plastics and Electrical Insulating Materials. :12 Doi: 10.1520/D0790-17.

[50] M. Bodaghi, A. Serjouei, A. Zolfagharian, M. Fotouhi, H. Rahman, D. Durand, Reversible energy absorbing meta-sandwiches by FDM 4D printing, Int. J. Mech. Sci. 173 (2020) 105451, https://doi.org/10.1016/j.ijmecsci.2020.105451.

[51] E. Soleyman, D. Rahmatabadi, K. Soltanmohammadi, M. Aberoumand, I. Ghasemi, K. Abrinia, M. Baniassadi, K. Wang, M. Baghani, Shape memory performance of PETG 4D printed parts under compression in cold, warm, and hot programming, SMS 31 (8) (2022) 85002, https://doi.org/10.1088/1361-665X/ac77cb.

[52] Z. Hou, X. Tian, J. Zhang, D. Li, 3D printed continuous fibre reinforced composite corrugated structure, Compos. Struct. 184 (2018) 1005–1010, https://doi.org/10.1016/j.compstruct.2017.10.080.

[53] P. Zhang, S. Sun, J. Duan, H. Fu, Z. Han, H. Geng, Y. Feng, Line width prediction and mechanical properties of 3D printed continuous fiber reinforced polypropylene composites, Addit. Manuf. 61 (2023) 103372, https://doi.org/10.1016/j.addma.2022.103372.

[54] W. Zhu, S. Li, Y. Peng, K. Wang, S. Ahzi, Effect of continuous fiber orientations on quasi-static indentation properties in 3D printed hybrid continuous carbon/kevlar fiber reinforced composites, Polymers for Adv. Technol. 34 (5) (2023) 1565–1574, https://doi.org/10.1002/pat.5991.

[55] S.F. Siddiqui, A. Archer, D. Fandetti, C. McGee, Cryogenic tensile performance of 3D printed onyx–continuous carbon fiber composites, Rapid Prototyp. J. (2023), https://doi.org/10.1108/RPJ-10-2022-0341.

[56] T. Cersoli, B. Yelamanchi, E. MacDonald, J.G. Carrillo, P. Cortes, 3D printing of a continuous fiber-reinforced composite based on a coaxial Kevlar/PLA filament, Compo. Adv. Mater. 30 (2021), https://doi.org/10.1177/26349833211000058.

[57] W. Liu, N. Wu, K. Pochiraju, Shape recovery characteristics of SiC/C/PLA composite filaments and 3D printed parts composites part A, Appl. Sci. Manufacturing 108 (2018) 1–11, https://doi.org/10.1016/j.compositesa.2018.02.017.

[58] P. Wu, T. Yu, M. Chen, D. Hui, Effect of printing speed and part geometry on the self-deformation behaviors of 4D printed shape memory PLA using FDM, J. Manuf. Process. 84 (2022) 1507–1518, https://doi.org/10.1016/j.jmapro.2022.11.007.

[59] M.L. Dezaki, A. Zolfagharian, F. Demoly, M. Bodaghi, Human-material Interaction enabled by fused filament fabrication 4D printing, Adv. Eng. Mater. (2024), https://doi.org/10.1002/adem.202301917.

[60] K.L. Ameta, V.S. Solanki, S. Haque, V. Singh, A.P. Devi, R.S. Chundawat, Critical appraisal and systematic review of 3D & 4D printing in sustainable and environment-friendly smart manufacturing technologies, Sustain. Mater. Technol. 34 (2022) e00481, https://doi.org/10.1016/j.susmat.2022.e00481.

[61] WT. Nugroho, Y. Dong, A. Pramanik, J. Leng, S. Ramakrishna, Smart polyurethane composites for 3D or 4D printing: general-purpose use, sustainability and shape memory effect, Compos. B Eng. 223 (2021) 109104, https://doi.org/10.1016/j.compositesb.2021.109104.

[62] M. Javaid, A. Haleem, Significant advancements of 4D printing in the field of orthopaedics, J. Clinical Orthopaedics and Trauma 11 (Suppl 4) (2020) S485–S490, https://doi.org/10.1016/j.jcot.2020.04.021.

[63] A. Zolfagharian, M.T. Gregory, M. Bodaghi, S. Gharaie, P. Fay, Patient-specific 3D-printed splint for mallet finger injury, Int. J. bioprinting 6 (2) (2020) 259, https://doi.org/10.18063/ijb.v6i2.259.

[64] M. Kaur, S.M. Han, W.S. Kim, Three-dimensionally printed cellular architecture materials: perspectives on fabrication, material advances, and applications, MRS Commun. 7 (1) (2017) 8–19, https://doi.org/10.1557/mrc.2016.62.

[65] A. Nazir, K.M. Abate, A. Kumar, J. Jeng, A state-of-the-art review on types, design, optimization, and additive manufacturing of cellular structures, Int J Adv Manuf Technol 104 (9–12) (2019) 3489–3510, https://doi.org/10.1007/s00170-019-04085-3.

[66] SH. Siddique, PJ. Hazell, H. Wang, JP. Escobedo, AAH. Ameri, Lessons from nature: 3D printed bio-inspired porous structures for impact energy absorption – a review, Addit. Manuf. 58 (2022) 103051, https://doi.org/10.1016/j.addma.2022.103051.

[67] C.W. Isaac, F. Duddeck, Current trends in additively manufactured (3D Printed) energy absorbing structures for crashworthiness application - a review, Virtual and Physical Prototyping 17 (4) (2022) 1058–1101, https://doi.org/10.1080/17452759.2022.2074698.

[68] A. Ghazlan, T. Nguyen, T. Ngo, S. Linforth, V.T. Le, Performance of a 3D printed cellular structure inspired by bone, Thin-Walled Struct. (2020) 106713, https://doi.org/10.1016/j.tws.2020.106713.

[69] SASA. Saufi, MYM. Zuhri, ML. Dezaki, SM. Sapuan, RA. Ilyas, A. As'arry, MKA. Ariffin, M. Bodaghi, Compression behaviour of bio-inspired honeycomb reinforced starfish shape structures using 3D printing technology, Polymers 13 (24) (2021) 4388, https://doi.org/10.3390/polym13244388.

[70] M. Bodaghi, N. Namvar, A. Yousefi, H. Teymouri, F. Demoly, A. Zolfagharian, Metamaterial boat fenders with supreme shape recovery and energy absorption/dissipation via FFF 4D printing, SMS 32 (9) (2023) 95028, https://doi.org/10.1088/1361-665X/acedde.

[71] H. Yin, W. Zhang, L. Zhu, F. Meng, J. Liu, G. Wen, Review on lattice structures for energy absorption properties, Compos. B Eng. 304 (2023) 116397, https://doi.org/10.1016/j.compstruct.2022.116397.

[72] R. Hedayati, A. Yousefi, M. Bodaghi, Sandwich structures with repairable cores based on truncated cube cells, Compo. Part B: Eng. 243 (2022) 110124, https://doi.org/10.1016/j.compositesb.2022.110124.